Journal of Photochemistry and Photobiology A: Chemistry 270 (2013) 43–52

Contents lists available at ScienceDirect

Journal of Photochemistry and Photobiology A: Chemistry

journal homepage: www.elsevier.com/locate/jphotochem

Photo-isomerization upshifts the pK_a of the Photoactive Yellow Protein chromophore to contribute to photocycle propagation

Sadia Naseem[a,1], Adèle D. Laurent[b,1], Elizabeth C. Carroll[a], Mikas Vengris[d], Masato Kumauchi[c], Wouter D. Hoff[c], Anna I. Krylov[b], Delmar S. Larsen[a,*]

[a] Department of Chemistry, University of California, Davis, One Shields Avenue, Davis, CA 95616 USA
[b] Department of Chemistry, University of Southern California, Los Angeles, CA 90089-0482, USA
[c] Department of Microbiology & Molecular Genetics, Oklahoma State University, Stillwater, OK 74078, USA
[d] Quantum Electronics Department, Faculty of Physics, Vilnius University Sauletekio 10, LT10223 Vilnius, Lithuania

ARTICLE INFO

Article history:
Received 11 March 2012
Received in revised form 19 June 2013
Accepted 25 June 2013
Available online 9 July 2013

Keywords:
Photoactive Yellow Protein
Photoisomerization
Quantum Modeling
Photoreceptors
Para-coumaric acid

ABSTRACT

The influence of chromophore structure on the protonation constant of the Photoactive Yellow Protein chromophore is explored with isolated *para*-coumaric acid (*p*CA) and thiomethyl-*para*-coumaric acid model chromophores in solution. pH titration coupled with visible absorption spectra of the *trans* and photogenerated *cis* conformer of isolated *p*CA demonstrates that the isomerization of the chromophore increases the pK_a of the phenolate group by 0.6 units (to 10.1 ± 0.22). Formation of the *p*CA thioester reduces the pK_a of the phenolic group by 0.3 units (from 9.5 ± 0.15 to 9.2 ± 0.16). Unfortunately, a macroscopic *cis*-TM*p*CA population was not achieved via photoexcitation. Both trends were explained with electronic structure calculations including a Natural Bond Orbital analysis that resolves that the pK_a upshift for the *cis* configuration is attributed to increased Columbic repulsion between the coumaryl tail and the phenolate moieties. This structurally induced pK_a upshift after isomerization is argued to aid in the protonation of the chromophore within the PYP protein environment and the subsequent propagation of the photocycle response and in vivo photo-activity.

1. Introduction

Photosensory receptor proteins transduce photon energy into physiological function and play essential roles for most organisms to adjust their behavior and metabolism in response to the quantity and quality of light in their environment [1]. These proteins operate by the photoexcitation of small molecular chromophores bound within complex protein scaffoldings; the excitation of which initiate light-dependent structural changes in the surrounding protein and ultimately trigger signal phototransduction pathways [2,3]. Photoreceptors are also ideal systems to study the molecular-level basis for structure-function relationships since they share similar structural motifs with more ubiquitous non-light activating signal transducion proteins and can be triggered with short pulses of light to synchronously observe their signaling activity [2,4,5]. One such photoreceptor is the Photoactive Yellow Protein (PYP), which is a small 125 amino acid-containing water-soluble protein found in the bacterium *Halorhodospira halophila* and is responsible for triggering the negative phototactic response of the organism to blue light [6–8].

The underlying photophysics of PYP is complex with a broad range of chemical reactions participating in its photoresponse. Photo-excitation of the dark-adapted pG state of PYP induces a rapid (<2 ps) *trans/cis* isomerization around a double bond of the internally bound *p*-coumaric acid molecule (*p*CA) [8–17] that is covalently bound to the sole cysteine residue of the protein (Cys49) through a thioester bond (Fig. 1A). This, in turn, initiates a complicated series of reversible reactions extending over 15 decades in time from femtoseconds to seconds [18–21] that involve chromophore protonation (Fig. 1B and C) [18,22], protein unfolding, and hydrogen-bond disruption [23,24], followed by the corresponding recovery reactions to complete a photocycle by reforming pG. Due to the simplicity of PYP's single-domain protein structure, it is an excellent system for studying the complex relationship between protein dynamics and chemical reaction dynamics and more specifically how nature has tuned both to generate photobiological activity. One relationship of particular interest is resolving how photoexcitation initiates and propagates the PYP photocycle (Fig. 2A) and specifically how chromophore isomerization facilitates the proton transfer reactions that are critical for PYP photoactivity. To understanding this, the detailed knowledge of the

* Corresponding author. Tel.: +1 5307526507.
E-mail address: dlarsen@ucdavis.edu (D.S. Larsen).
[1] These authors contributed equally to this manuscript.

1010-6030/$ – see front matter © 2013 Elsevier B.V. All rights reserved.
http://dx.doi.org/10.1016/j.jphotochem.2013.06.019

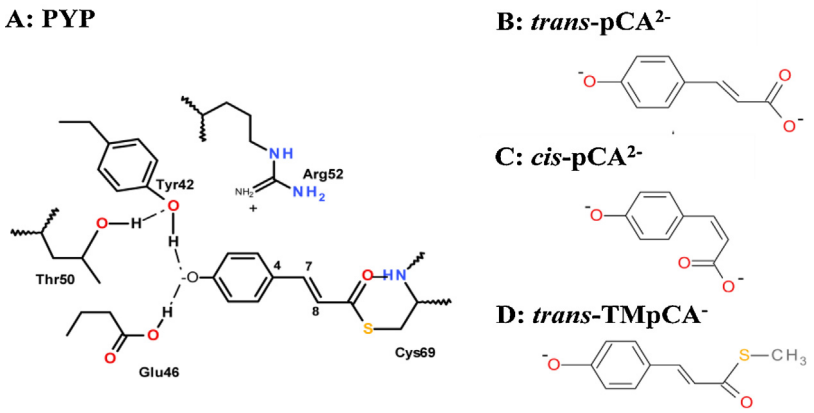

Fig. 1. Molecular structures of studied PYP chromophores. (A) the protein-bound *trans*-PYP chromophore in the ground state (pG). (B) *trans*-*p*CA^{2-} at high pH (fully deprotonated), (C) *cis*-*p*CA^{2-} at high pH (fully deprotonated) and (D) *trans*-TM*p*CA^{-} at high pH (deprotonated).

interactions between structure, protonation, and electronic structure must be resolved.

When bound to the PYP protein, the *p*CA chromophore is sterically constrained by the surrounding protein nanospace, which includes hydrogen bonds with several amino acids (Glu46 and Tyr42 on the phenolate side and Cys49 on the carbonyl side). Furthermore, the *p*CA chromophore is also influenced by electrostatic interactions with nearby residues, especially the guanidinium cation of Arg52 (Fig. 1A) [25]. Protonation of *p*CA within the protein occurs via the donation of a labile proton from Glu46, although Tyr42 also participates in the hydrogen bonding to *p*CA [18,22,26], which induces a partial unfolding (ms) of the protein and the formation of the pB signaling state (Fig. 2A) [22,27,28]. A simple scheme describing this reaction (Fig. 2B) involves a potential energy surface with the proton originally located on E46 (left well) that is coerced to *p*CA (right well) over an energy barrier $\Delta G^{\ddagger}$ (blue components) [29,30]. Multiple factors facilitate this reaction within PYP including the making and breaking of hydrogen bonding and evolution on the excited-state surface [31–35], which also involve individual bond angles and distances, fluctuations, energetics (both local and long range), and the intrinsic proton affinities of Glu46 (donor) and *p*CA (acceptor) molecules [25,36,37]. The last contribution results from the electron distributions within the donor and acceptor, which contribute to the Gibbs free energy difference (ΔG) for the protonation reaction and is often discussed in terms of constituent protonation pK_a values for the species at least for solvent exposed species.

Consequentially, electronic structure, chromophore deformation, and protonation intermix to activate and propagate the PYP photocycle and are strongly modulated by the detailed interactions between pCA and the surrounding protein scaffolding. The underlying chromophore properties can be resolved by removing the complexities of the protein environment and studying the isolated chromophore properties in solution. Here, we investigate the effect of chromophore conformation on the the pK_a of the PYP chromophore by exploring the structure- induced protonation properties of two model chromophores outside of the PYP protein environment: *p*CA and its thiomethyl ester analog, TM*p*CA (Fig. 1D). The pK_a values of the *trans* and *cis* forms of *p*CA were resolved in vitro after photo-irradiation and were compared to high-level ab initio electron structure calculations to provide insight into the electron charge distributions for the different conformations and how they affect the pK_a values.

2. Experimental and computational details

Trans-*p*CA and HPLC grade water were purchased from Sigma-Aldrich and used as received. The synthesis of TM*p*CA involved adding 10 ml of a DMF solution of *trans p*-coumaric acid (3-(4-hydroxy-phenyl) acrylic acid; Aldrich) (2.00 g) to 10 ml DMF solution of DCC (*N*,*N*′-dicyclohexylcarbodiimide; Pierce) (1.24 g) under magnetic stirring. The mixture was incubated at 90 °C for 1 h, resulting in a *p*-coumaric acid anhydride solution with a characteristic pale yellow color. Precipitated *N*,*N*′-dicyclohexylurea, which

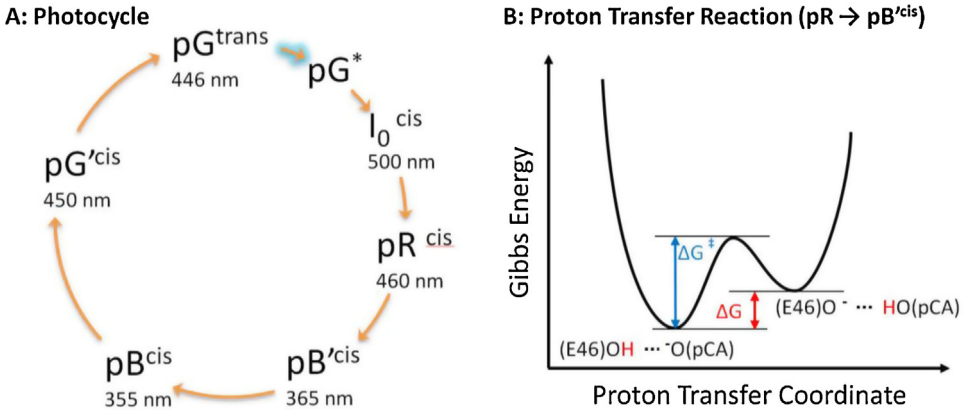

Fig. 2. (A) PYP photocycle indicating the dark-adapted state (pG), the light-adapted state (pB), and photointermediates. The isomerization states of the p-coumaric acid chromophore are denoted. The pB intermediates have a protonated chromophore, while pG, I_0, and pR intermediates are deprotonated. (B) Free energy profile for the proton transfer reaction involved in formation of the pB′ signaling state from pR.

was produced during the formation of the acid anhydride, was removed by centrifugation (5500 × *g*, 10 min) and the resulting pale yellow solution was added to 5 ml of a DMF suspension containing sodium methanethiolate (Fluka) (1.00 g) under vigorous stirring. The resulting orange mixture was extracted with ethyl acetate and washed three times with an aqueous solution of NH_4Cl and then washed three times with H_2O. The solution was dried over $MgSO_4$ and evaporated in vacuo. The residual yellow oil was dissolved in 5 ml of ethyl acetate and chromatographed on silica-gel (Sigma–Aldrich) with hexane and ethyl acetate (from 4:1 to 1:1 (v/v)) as the eluent. After recrystallization from ether, 235 mg of pale yellow crystals was obtained with a yield of 20%. The structure and purity of the compound was confirmed by NMR spectroscopy: ^{1}H-NMR (400 MHz, CD_3OD, TMS) δ 2.3 (s, 3H, CH_3), 6.60 and 6.64 (d, ^3J = 15.6 Hz, 1H, H-C_α), 6.76 and 6.79 (d, ^3J = 8.4 Hz, 2H, H-$Ph_{3,5}$), 7.42 and 7.44 (d, ^3J = 8.4 Hz, 2H, H-$Ph_{2,6}$), 7.49 and 7.53 (d, ^3J = 15.6 Hz, 1H, H-C_β).

A mercury lamp (ORIEL 68806) with either a 335-nm or 365-nm band-pass interference filter was used to illuminate solutions of *trans*-*p*CA and *trans*-TM*p*CA; a second illumination study of TM*p*CA was also performed with a continuous-wave 446-nm LED array (Roithner Labs, Austria L435-66-60-550). The absorption spectra of illuminated solutions were measured at different pH values (7-12.5) and pK_a values were estimated from the decomposition into constituent populations with different protonation states (using static absorption spectra as a basis). The resulting *cis*-*p*CA solution exhibited no signs of degradation or thermal back conversion to the *trans* conformation when kept at room temperature in the dark (not shown). Aqueous solutions of *p*CA were prepared with 0.05 M KOH to ensure full deprotonatation and solutions of TM*p*CA were prepared at pH 11 with a phosphate buffer to avoid hydrolysis of the thioester linkage; both were prepared with an optical density of ∼1 per mm at the peak of the absorption spectrum. The absorption spectra were monitored as the pH of aqueous solutions was adjusted drop wise with concentrated HCl and KOH stock solutions and the same procedure was adopted with *cis*-*p*CA and *trans*-TM*p*CA. pH values were measured with an Acorn pH Meter (Oakton WD-35613-00) and all titration curves were repeated four times to ensure reproducibility.

The energies, equilibrium geometries, vibrational frequencies were computed at the ωB97X/6-31+G(d,p) level of theory. No imaginary frequencies were detected for the optimized structure of the *trans* *p*CA model at all protonation states and one imaginary frequency was detected for mono-deprotonated *cis*-*p*CAH$^-$ that disappeared when the fully optimized structure was allowed to deviate from a planar geometry. For TM*p*CA, the basis set for the calculations was extended to 6-31+G(2df,p) to include polarization functions for the sulfur atom in the thioester of the coumaryl tail (Fig. 1D). The carefully re-parameterized ωB97X functional, which includes a long-range correction to mitigate notorious self-interaction errors, demonstrates superior performance relative to the B3LYP functional (e.g., as observed in the root-mean square errors of proton affinities of 1.72 kcal/mol) [38]. The optimized structures of all studied protonation states and isomers of TM*p*CA and *p*CA chromophores in the gas phase were planar, with the exception of *cis*-*p*CAH$^-$. Charge distributions were analyzed with Natural Bond Orbital analysis [39]. All calculations were performed with the Q-Chem electronic structure package [40].

3. Experimental results

The photodynamics and static properties of several PYP chromophore analogs have been previously studied outside the protein including *p*CA [41], thio-methyl-*p*-coumaric acid (TM*p*CA) [42] and others (Fig. 1) [11,43–46]. Isolated *p*CA (both *trans* and *cis* configurations) in solution can exist in three different protonation states

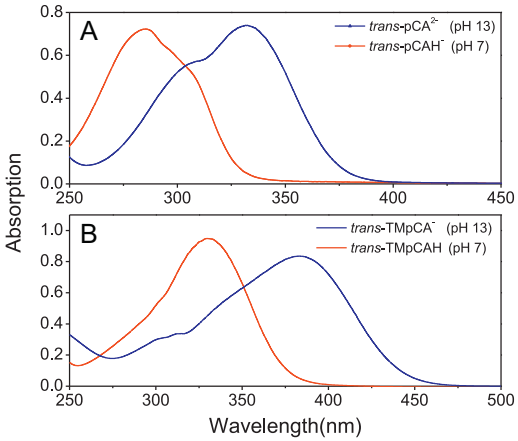

Fig. 3. pH dependent absorption spectra. (A) The *trans*-*p*CA spectra of the singly-protonated pH = 7 form (red line) and the doubly-protonated pH = 13 form (blue line) peak at 280 nm and 330 nm, respectively. (B) *trans*-TM*p*CA in water at the same pH values used in panel A. (For interpretation of the references to color in this figure legend, the reader is referred to the web version of the article.)

depending on the protonation of the carboxylic acid and/or the phenolic moieties [47], which can be easily identified in the electronic absorption spectra (Fig. 3). The singly-deprotonated, neutral pH, *p*CAH$^-$ state exhibits an absorption at 285 nm (4.35 eV) and the subsequent deprotonation of the phenolic group at higher pHs results in a red-shifted absorption at 332 nm (3.74 eV) for *p*CA^{2-}. The sensitivity of the absorption spectrum to the protonation states of the chromophore indicates that the charge on the phenolic oxygen significantly alters the electron density distribution in the molecule [47–49]. Only the phenolate deprotonation reaction (*p*CA^{2-}/*p*CAH$^-$ and TM*p*CA$^-$/TM*p*CA) was investigated further with pH titrations since it is the biologically relevant protonation reaction in initiating and propagating the PYP photocycle.

The methyl group in TM*p*CA acts as an inert, small capping group that hinders the observed dynamics less than would be expected with larger, bulkier groups [11,50]. TM*p*CA$^-$ in aqueous solution has a spectrum that is appreciably red shifted (380 nm or 3.36 eV) compared to *p*CA^{2-} (335 nm or 3.70 eV) and is closer to wild-type PYP's absorption spectrum peaking at 446 nm (2.78 eV) [47]. Both TM*p*CA and wildtype-PYP exhibit similar excited-state quenching kinetics (∼2 ps) and TM*p*CA exhibits high photostability [51].

The static absorption spectra in Fig. 4 exhibit photo-stationary equilibria established from irradiating *trans*-*p*CA^{2-} (pH 12) and *trans*-TM*p*CA$^-$ (pH 11) and are in agreement with the known spectral changes associated with *cis*/*trans* isomerization for *p*CA^{2-} [52], with the *cis* spectrum exhibiting a blue shifted and decreased amplitude absorption. An isosbestic point at 298 nm is observed in the dynamics, indicative of two-population kinetics (i.e., *trans* and *cis* isomers). Both protonation states of *p*CA demonstrate photoisomerization activity with the *cis* isomers exhibiting a blue-shifted absorption (Fig. 4A) relative to the *trans* isomer for pH = 7 and pH = 12 solutions (low pH spectra not shown). In contrast to *p*CA^{2-}, irradiation of *trans*-TM*p*CA$^-$ (at 365-nm) did not produce a stable *cis* photoproduct and continued irradiation eventually degraded the *trans* isomer into a final photoproduct that resembles free phenolate ions (or phenol) in solution (Figs. S2 and S3) [53]. A 445-nm LED array was also used to excite the low energy red tail of the *trans*-TM*p*CA$^-$ absorption spectrum and no significant isomerization was observed (even after 10 h irradiation). Neutral TM*p*CA also appeared to undergo rapid photodegradation rather than simple photoisomerization (Fig. S2). The irradiation did not photoconvert 100% of the *trans*-pCA molecules to the *cis* conformation in solution, which was estimated at 84% based on the amplitude of the red-most absorption band.

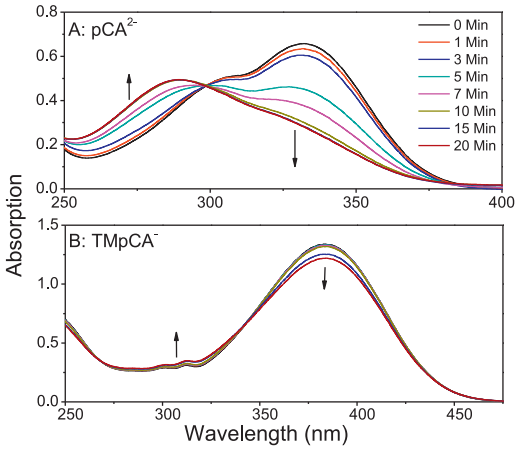

Fig. 4. Absorption spectra after 365-nm illumination. (A) *trans* pCA^{2-} acid at pH = 12. (B) *trans*-TM*p*CA^{-} at pH 11. Spectra for both samples are color coded to the different exposure durations (indicated in panel A). (For interpretation of the references to color in this figure legend, the reader is referred to the web version of the article.)

The pK_a values for the *trans* and *cis* protonation reactions of pCA^{2-}/$pCAH^{-}$ and *trans* TM*p*CA^{-}/TM*p*CA are directly estimated from the titration curves in Fig. 6. The *trans* and *cis*-*p*CA absorption spectra (Fig. 5) are used as basis spectra to decompose the pH-dependent absorption spectra monitored during titration to determine the concentrations of single-deprotonated ($pCAH^{-}$) and double-deprotonated populations (pCA^{2-}). The pK_a values are then estimated by fitting the pH-dependent concentration profiles (e.g., α_a for $pCAH^{-}$ and α_b for pCA^{2-}) to the sum of Henderson-Hasselbalch approximations for the irradiated (i.e., *cis*/*trans* occupation ratio at 84/16%) and non-irradiated samples (*cis*/*trans* occupation ratio at 0/100%):

$$\alpha_a = \frac{1}{1 + 10^{\mathrm{pH}-\mathrm{p}K_a}} \quad \text{and} \quad \alpha_b = 1 - \alpha_a \tag{5}$$

under the assumption that the protonation of the carboxylic group (p$K_a \sim 3$) can be neglected in this pH range (7–12). The *trans*-*pCA* and *cis*-*p*CA exhibit different pK_a values of 9.5 ± 0.15 (standard deviation) and 10.1 ± 0.22, respectively (Fig. 6A). Thiomethylation of the carboxylic group in TM*p*CA (Fig. 1C) decreases the phenolic pK_a for the *trans* isomer to 9.2 ± 0.15 (Fig. 6B). Unfortunately, the pK_a for the *cis* isomer of TM*p*CA could not be resolved since a macroscopic *cis*-TM*p*CA population could not be generated (Fig. 4B).

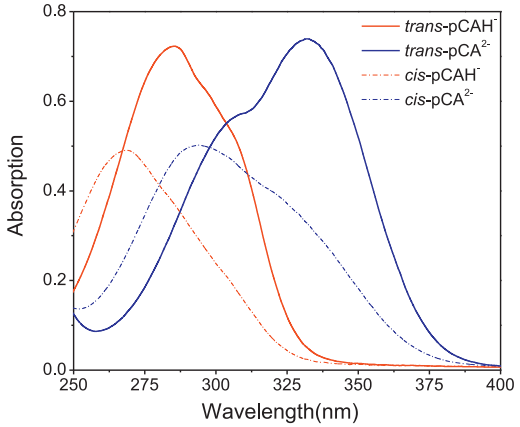

Fig. 5. Initial and final absorption spectra for pCA^{2-} (blue curves, pH 13) and $pCAH^{-}$ (red curves, pH 7). The *trans* (solid lines) and *cis* spectra (dashed lines) for each protonation state are estimated from the 180 minutes of illumination with 365-nm light. (For interpretation of the references to color in this figure legend, the reader is referred to the web version of the article.)

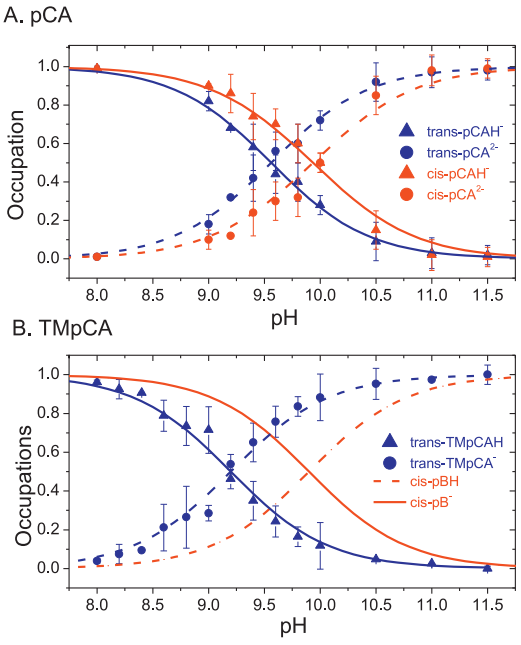

Fig. 6. Occupation plots from the titration curves for *trans* (blue circles) and *cis* (red circles) isomers of the chromophores. (A) The titration curves of aqueous *p*CA with protonated $pCAH^{-}$ (solid lines) and deprotonated pCA^{2-} (dashed lines) with an estimated pK_a of 9.5 ± 0.18 for *trans*-*p*CA and 10.1 ± 0.23 for *cis*-*p*CA. (B) The titration curves of aqueous *trans*-TM*p*CA with protonated *trans*-TM*p*CAH (solid lines) and deprotonated *trans*-TM*p*CA^{-} (dashed lines) with an estimated pK_a of 9.2 ± 0.15 for *trans*-TM*p*CA are estimated from the fit of the Henderson–Hasselbalch approximation to the data (Eq. (5)). For comparison, the estimated pK_a of the PYP chromophore in the solvent exposed pB state is shown (as labeled in legend) [54]. (For interpretation of the references to color in this figure legend, the reader is referred to the web version of the article.)

However, for comparison, the estimated pK_a of the PYP in the solvent exposed pB state of wild-type PYP by Hellingwerf and co-workers is shown [54].

4. Quantum chemical modeling

Connecting these experimental results to pKa values computed with ab initio methods requires accurate determination of the Gibbs free energy difference in solution (ΔG_{sol}) of the underlying deprotonation reaction:

$$\mathrm{p}K_a = \frac{\Delta G_{\mathrm{sol}}}{2.303\,RT} \tag{1}$$

where *T* is temperature and R is the gas constant. Several methodologies have been developed to compute the variation of the Gibbs free energy in solution (ΔG_{sol}) including MD simulations and the free-energy perturbation approach [55], QM/MM schemes [56–58], and ab initio calculations [59].

To model the solvent, high level ab initio theory is often combined with implicit solvation models such as SS(V)PE [60,61], COSMO [62], C-PCM [63], SM8 [64], etc., which differ in the expression of the electrostatic interaction and other empirical parameters such as the choice of the cavity around the solute, and the dispersion and repulsion terms of solvent-solute interaction. The thermodynamic cycle shown in Fig. 7 is used to compute ΔG_{sol} with a general deprotonation reaction ($AH \rightarrow A^{-} + H^{+}$), whereby ΔG_{sol} is determined via the following equation:

$$\Delta G_{\mathrm{sol}} = \Delta G_{\mathrm{g}}^{(\mathrm{AH}^{-}/A)} + \Delta G_{\mathrm{aq}}^{A-} + \Delta_{\mathrm{aq}}^{H^{+}} - \Delta G_{\mathrm{aq}}^{\mathrm{AH}} \tag{2}$$

The first term on the right side of the equation is the gas phase Gibbs energy difference between the protonated form (AH) and deprotonated form (A^{-}) of the solute, usually computed with the

Table 1
Gas phase electronic energy (ΔE), internal energy (ΔU) and Gibbs free energies (ΔG) differences between the deprotonated and protonated states of the *trans* and *cis* forms of the two model systems. All energies are given in kcal/mol. The level of theory is ωB97X/6-31+G(d,p) for *p*CA and ωB97X/6-31+G(2df,p) for TM*p*CA. ΔpK_a values are computed using gas phase ΔE and ΔU by Eq. (4).

Chromophore models	*trans*			*cis*			ΔpK_a (from $\Delta\Delta E$)	ΔpK_a (from $\Delta\Delta U$)	ΔpK_a(from $\Delta\Delta G$)
	ΔE	ΔU	ΔG	ΔE	ΔU	ΔG			
TM*p*CAH/TM*p*CA$^-$	338.67	329.96	330.31	339.95	331.17	331.34	−0.94	−0.89	−0.75
*p*CAH$^-$/*p*CA^{2-}	402.62	394.29	393.62	410.11	401.67	401.71	−5.49	−5.40	−5.92

zero-point vibrational energy correction (ZPE). ΔG_{aq}^{A-} is the difference of the free Gibbs energy going from the gas phase to the aqueous phase and can be computed with the implicit solvation models described above. In particular, the SM8 model developed by Truhlar has been shown to be reliable in computing ΔG_{aq} with a mean unsigned deviation of 0.59 kcal/mol for neutral compounds and 4.55 kcal/mol for anionic species [64]. Since an error of 1.36 kcal/mol in G_{aq} results in a one pH unit error in pK_a (Eq. (1)), the accurate determination of the solvation energies for all species is important. For the hydrated proton (ΔG_{aq}^{H+}), the currently accepted value of −264.0 kcal/mol at 1 atm and 1 M was used [65].

Useful information regarding the isomerization effects can be gleaned from relative comparisons and ratios of calculated values, especially of the non-solvated gas-phase species. Table 1 collects electronic energy (ΔE), internal energy (ΔU), and Gibbs free energy (ΔG) differences for protonated and deprotonated forms of the *cis* and *trans* PYP chromophore models in the gas phase. The difference in pK_a values between the *cis* and *trans* isomers (ΔpK_a) can be expressed as the difference of Gibbs free energy differences ($\Delta\Delta G$) for the respective deprotonation reactions (Fig. 2B). The dominant contribution to $\Delta\Delta G$ is the gas phase energy difference, $\Delta\Delta E$ (or internal energy difference, $\Delta\Delta U$, when ZPE is included:

$$\Delta\Delta E = \Delta E_{trans} - \Delta E_{cis} \quad (3)$$

where ΔE_{trans} and ΔE_{cis} are the energy differences between the deprotonated and protonated phenol moiety of the *trans* and *cis* PYP chromophore models, respectively (Table 1).

The gas phase calculations provides a useful probe into the factors that affect ΔpK_a (without having to calculate error-prone solvation energies), which can be evaluated as follows:

$$\Delta pK_a = \frac{\Delta\Delta G}{2.303RT} \approx \frac{\Delta\Delta E}{2.303RT} \quad (4)$$

As Table 1 demonstrate, ΔG differs from ΔU by less than 1 kcal/mol indicating that differences in ΔG between *cis* and *trans* isomers (and ΔpK_a) are largely dominated by the electronic energy difference (ΔE) and that entropic and enthalpic contributions almost entirely cancel. Table 2 focuses on the respective energy differences between *cis* and *trans* forms of the chromophores. The solvation energies, which are also necessary for computing absolute pK_a, are given in the Supplementary Information (Table S1). Finally, Table 3 compares the computed and experimental values of pK_a of the chromophores.

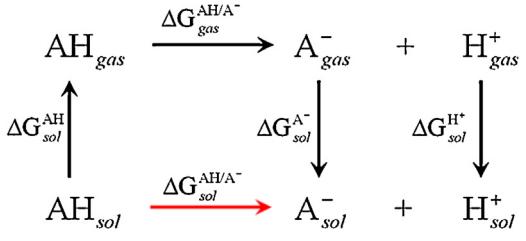

Fig. 7. The thermodynamic cycle used to compute the Gibbs free energy changes in aqueous solution, ΔG_{sol}.

Table 2
Gas phase energy differences between the *trans* and *cis* forms for each species in this study. All energies are given in kcal/mol. The level of theory is ωB97X/6-31+G(d,p) for *p*CA and ωB97X/6-31+G(2df,p) for TM*p*CA.

Species	$E_{trans} - E_{cis}$	$U_{trans} - U_{cis}$	$G_{trans} - G_{cis}$
TM*p*CAH	−4.63	−5.13	−5.56
TM*p*CA$^-$	−5.19	−6.34	−6.59
*p*CAH$^-$	−2.01	−2.34	−1.61
*p*CA^{2-}	−9.50	−9.72	−9.70

5. Discussion

pK_a values are important determinants of biomolecular (particularly enzymatic) function and can be used to assess functional activity and identify active sites. However, estimating pK_a values is often difficult, both experimentally and theoretically. The experimental methods available for estimating pK_a values of buried amino acids or prosthetic groups in proteins are either indirect (e.g., resolving the pH dependence of kinetics such as k_{cat} in enzymes) or direct (following the ionization of a single residue via spectroscopy in a pH titration) [66,67]. Unfortunately, the former is not applicable in many samples (including PYP) and the latter can be greatly obscured by the other ionizable groups in large proteins. Moreover, pK_a values can be estimated with computational algorithms from known protein X-ray structures, however, these approaches are largely optimized for amino acid residues and are not easily applicable to prosthetic groups like *p*CA in PYP [16,68]. Extending these studies to resolve the pK_a values of transient populations (e.g., Fig. 2A) in the protein is even more difficult to realize.

Although the pH of the buffer solution in which the PYP protein is dissolved can be varied and its effect on the *p*CA chromophore can be spectroscopically monitored, correlating such external titration data to the internal pK_a (i.e. proton affinity) of the PYP chromophore is complicated by the limited accessibility of the solvent to the chromophore. For example, the pK_a estimated for the isolated *trans*-*p*CA chromophore in aqueous solutions (Fig. 1B) is 9.5 [69–71]. However, in the dark-adapted pG state of wild type PYP, the chromophore remains deprotonated in aqueous solutions with pH values down to 3, at which the protein denatures and the chromophore is exposed to the solvent [72,73]. For I_0 and pR, the next intermediates in the photocycle (Fig. 2A) with an isomerized *p*CA, the pK_a values are unknown [74,75]. However, for the subsequent states (pB′ and pB), the *cis* chromophore is protonated with Glu46 deprotonated and the observed pK_a is 9.9 [54], which is in better agreement the isolated *trans*-*p*CA value. Since solvent access

Table 3
The computed (in solution) and experimental pK_a values between the *trans* and *cis* conformations.

Chromophore models	Isomer	pK_a^{exp}	pK_a^{calc}
TM*p*CA	trans	9.2 ± 0.16	13.47
	cis	n/a	13.67
pB	cis	9.9[a]	n/a
*p*CA	trans	9.5 ± 0.15	10.20
	cis	10.1 ± 0.22	10.82

[a] Estimated pK_a of the PYP chromophore in the solvent exposed pB state [54].

is important for titration studies, we use isolated model chromophores in solution instead to explore the pK_a values and how the chromophore structure influences them.

Although photo-isomerization is a commonly observed mechanism in the primary and secondary responses of many photosensory proteins [2,3], its role in initiating and propagating the photocycle dynamics is not yet fully understood. The interplay between isomerization, protonation and photoreceptor activity was discussed by Warshel in his seminal work on the bacteriorhodpsin (bR) photoactive protein [76], who proposed that the photo-isomerization of the retinal chromophore bound to bR induces a pK_a shift to drive the proton pumping activity of the system. This hypothesis was recently revised to argue that site-specific protein–retinal interactions between the different isomers must also be considered [77]. Later, Ottolenghi and Sheves suggested that only a charge redistribution or repolarization is required to initiate the bR photocycle and that the isomerization of the retinal chromophore is only a secondary effect [78]. A similar observation was demonstrated by Hellingwerf and co-workers who showed that the PYP photocycle can be weakly activated when the pCA chromophore is substituted with a fully locked analog, whereby isomerization is completely blocked [79].

The titration measurements in Fig. 6 estimate a pK_a for *trans*-*p*CA (9.5 ± 0.15) that is in agreement with previous measurements (9.35) [69–71]. Upon removal of all substitutions to the benzene ring (i.e., for bare phenol), the pK_a upshifts to 9.89 due to the absence of the inductive withdrawing capacity of the coumaryl tail [69,80]. To understand why the coumaryl tail preferentially upshifts the pK_a for the *cis* vs. *trans* conformer (by 0.6 pH units), we turn to quantum chemical calculations. A 0.6 pH upshift in pK_a equates to a less than 1 kcal/mol energy in the Gibbs free energy difference (Eq. (1)), which is difficult to reproduce quantitatively (especially due to errors in solvation energies) with typical error bars of electronic structure calculations [64].

The calculated ΔG_{sol} and $\Delta\Delta G_{sol}$ (i.e., $\Delta G_{sol}(AH) - \Delta G_{sol}(A^-) - \Delta G_{sol}(H^+)$) values for each compound/conformer are given in Table S1. While the solvation energy is important for reproducing absolute pK_a values, the solvent stabilization for *cis* and *trans* isomers of TM*p*CA appear to be near identical. Thus, neglecting the solvent contributions does not strongly affect ΔpK_a of TM*p*CA. However, $\Delta\Delta G_{sol}$ for depronation reaction between the *cis* and *trans* forms of *p*CA is significant (6 kcal/mol). This provides a basis for explaining the observed pK_a difference between the *cis* and *trans* isomers of *p*CA with gas phase energy differences (ΔE or ΔU) that can be computed far more accurately because they do not depend on solvent models (Table 1). Although such calculations are not expected to give quantitatively accurate pK_a values, they provide a good starting point for interpreting the experimental data.

While TM*p*CA is arguably a better model for the PYP chromophore in solution than *p*CA, as it features the pCA-cysteine thioester moeity found in PYP protein, its poor photoconversion yield in solution does not allow for the determination of pK_a of the *cis* form like with *p*CA. This may result from two mechanisms: (1) a low or no photoisomerization quantum yield and (2) the *cis*-TM*p*CA$^-$ conformation is unstable and rapidly converts back to the *trans* form. Very weak photoisomerization is observed at high pH = 12 (Fig. 4B), which is in agreement with the ultrafast pump–dump–probe signals for TM*p*CA$^-$ that also exhibit weak isomerization yields (<2%) [81]. In contrast, *p*CA within PYP has a significantly higher photo-isomerization yield of ~33% [82]. Attempting to generate *cis*-TM*p*CAH at pH 7 is more successful (Figure S2) in forming the stable *cis*-form, although secondary photodegradation reactions occur to also generate free phenol absorbing at ~265 nm. In contrast to the solution phase attempts, the *cis* isomerized chromophore within PYP in the pB state can be readily generated and exhibits a pK_a of 9.9 [54]. The inability to form a stable *cis*-TM*p*CA$^-$ in solution from the deprotonated conformer suggests the *cis* configuration of the chromophore may be unstable when deprotonated and does not require "help" from the protein environment to return to the *trans*-configuration for the thermally activated photocycle. Hence, the primary job of the pG′ intermediate (Fig. 2) may be to maintain the chromophore in a deprotonated state long enough to allow it to re-isomerise to the *trans*-configuration in pG.

5.1. Interpretation of electronic structure calculations

The gas phase deprotonation energies (ΔE and ΔU) for the *trans* and *cis* isomer for each possible protonation pair of TM*p*CA and *p*CA are contrasted in Table 1 and Fig. 8. For the biologically relevant phenolate-deprotonation reaction for TM*p*CA/TM*p*CA$^-$ and *p*CAH$^-$/*p*CA^{2-} systems, ΔE_{trans} is smaller than ΔE_{cis}, which results in a negative ΔpK_a (*cis* isomer is more basic) in agreement with the titration measurements of Fig. 6 (Eqs. (3) and (4)). While TM*p*CA$^-$, TM*p*CA, and *p*CA^{2-} are planar in both *trans* and *cis* isomer configurations, *p*CAH$^-$ is non-planar in its *cis* form, with the oxygen atoms of COO$^-$ out of plane of the phenol ring and double bond by 53°, likely due to steric and Coulombic repulsion (Table S2). To compare ΔpK_a in TM*p*CA and in *p*CA, the energy differences between *trans* and *cis* forms for each species are given in Table 2. The energetics suggest that ΔpK_a in TM*p*CA is smaller than in *p*CA due to the gas phase energy differences. Morevoer, the energy gap between deprotonated and protonated TM*p*CA chromophores will be always lower in energy than the one for *p*CAH$^-$ and fully deprotonated *p*CA^{2-}, owing to a larger energy gap between the *trans* and *cis* forms of *p*CA^{2-} (9.5 kcal/mol). Since a stable *cis*-TM*p*CA population could not be generated in solution, this could not be confirmed experimentally.

The above gas-phase analysis was extended to include the surrounding solvent (water) via four nonspecific continuum models: IEF-PCM or SS(V)PE [60,61] (which are identical), COSMO [62], C-PCM [63], and SM8 [64]. The best agreement for the computed pK_a values with the experimental results was obtained for the SM8 method, especially with the Truhlar's M06-2X functional (Table 3). The pK_a shifts are well reproduced with the computed ΔpK_a values for TM*p*CA and *p*CA are −0.20 (Exp. −0.7) and −0.62 (Exp. −0.6), respectively; however, absolute values are less accurate. The best agreement is observed for *p*CA. Comparing ΔpK_a obtained from gas phase $\Delta\Delta G$ (Table 1) with ΔpK_a that includes the solvation effect (Table 3), we observe that the solvent has little effect on TM*p*CA (−0.75 vs. −0.20) due to the nearly identical $\Delta\Delta G_{sol}$ for the *trans* and *cis* isomers, while for *p*CA ΔpK_a decreases by 5 pH units (−5.92 to −0.6) due to the 6 kcal/mol solvent effect discussed above (Table S1 for $\Delta\Delta G_{sol}$).

To rationalize why the energy penalty for deprotonation is higher for *cis* isomers of TM*p*CA and *p*CAH$^-$, the electron charge distribution patterns were analyzed. Fig. 9 shows the Natural Bond Orbital charge distribution for TM*p*CA with three primary structural components: (1) phenol, (2) the methylene bridge and (3) the thiomethyl group (or carboxylate group for *p*CA). Somewhat surprisingly, isomerization does not considerably affect the charge distribution pattern with similar net charges of the three moieties observed (Table 4). However, the extra negative charge in the deprotonated species resides more on the phenolate and thiomethyl (or carboxylate) groups than on the bridge, hence the Coulomb repulsion between these two moieties *increases* upon deprotonation. Since these two groups are closer in the *cis* forms, we attribute the energy penalty for deprotonation to the larger Coulomb repulsion between the groups hosting excess charge in the *cis* relative to the *trans* isomers.

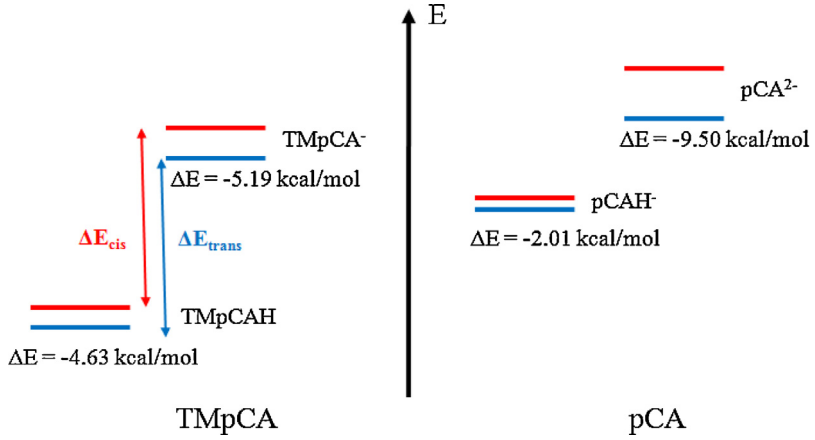

Fig. 8. Relative gas phase energies of the *cis* (red lines) and *trans* forms (blue lines) of TM*p*CA (left) and *p*CA (right) in different protonation states. Energy difference between *trans* and *cis* forms for each species is indicated as is the deprotonation energy (red vertical line for *cis* and blue vertical line for *trans*) for the TM*p*CAH/TM*p*CA$^-$ reaction (Table 2). (For interpretation of the references to color in this figure legend, the reader is referred to the web version of the article.)

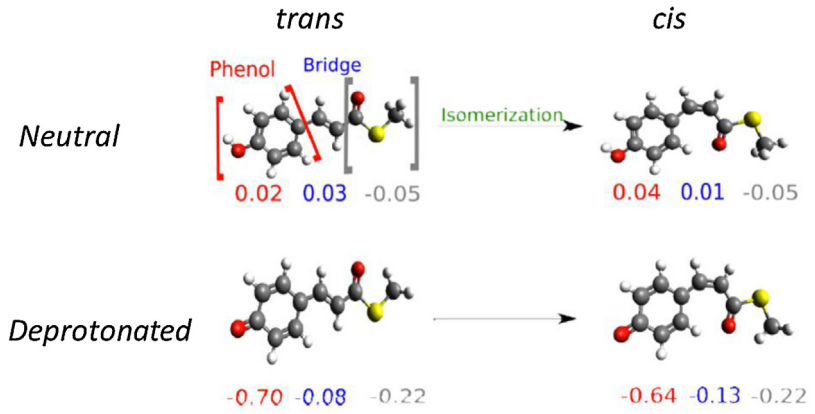

Fig. 9. Partial natural bond orbital charges of the three moieties (phenol, methylene bridge and thiomethyl) of the *trans* and *cis* isomers of TM*p*CA under neutral and deprotonated conditions.

5.2. Application to the PYP photocycle

Many factors influence the condensed phase proton transfer reactions within the highly organized protein scaffold. For *p*CA, important aspects include specific distance between residue and chromophore, fluctuation dynamics needed to promote energy barrier crossing ($\Delta G^{\ddagger}$ in Fig. 2B), and the inherent thermodynamics originating from the electronic structure (ΔG or pK_a) of the chromophore [25,37,83]. For PYP, the limited solvent access to *p*CA in the pG state complicates the traditional pK_a determination approaches, and the characterization of pK_a values for transient populations, i.e., pR is significantly more difficult to realize. To address this for the pre-protonation populations in PYP, we chose to study isolated model chromophores, which allows the experimental comparison of the solvent relaxed *trans* and *cis*-*p*CA molecules in solution to the *p*CA protein and provides a means to explore the electronic energy contribution to different conformations. Groenhof et al. proposed a similar pK_a upshift upon photo-isomerization of the PYP chromophore, which they predict to be appreciably twisted with a full break in the electronic conjugation between the phenolate moiety and the coumaryl tail [25]. This would upshift the pK_a to a value comparable to bare phenolate (9.89) [69]. However, our measurements and calculations clearly indicate that such a significant twist of pCA is unneeded to upshift the pK_a. This is supported by the near planar chromophore structures extracted from transient X-ray measurements on PYP by Ihee and co-workers demonstrating that the *p*CA is largely planar for the transient structures prior to protonation (Fig. 10 and Table S2) [84].

Table 4
Natural bond orbital (NBO) charge distributions for the *p*CA and TM*p*CA in gas phase. The differences between charges of the *cis* and *trans* forms are indicated in parentheses.

Chromophore models		Phenol(ate)	Bridge	$C(=O)SCH_3$/C(=O)O(H)
TM*p*CA	*trans*-TM*p*CAH	0.02 (+0.02)	0.03 (−0.02)	−0.05 (0.00)
	cis-TM*p*CAH	0.04	0.01	−0.05
	trans-TM*p*CA$^-$	−0.70 (+0.06)	−0.08 (−0.05)	−0.22 (0.00)
	cis-TM*p*CA$^-$	−0.64	−0.13	−0.22
*p*CA	*trans*-*p*CAH$^-$	−0.09 (+0.02)	−0.07 (−0.04)	−0.84 (+0.03)
	cis-*p*CAH$^-$	−0.07	−0.11	−0.81
	trans-*p*CA^{2-}	−0.97 (+0.03)	−0.13 (−0.05)	−0.90 (+0.02)
	cis-*p*CA^{2-}	−0.94	−0.18	−0.88

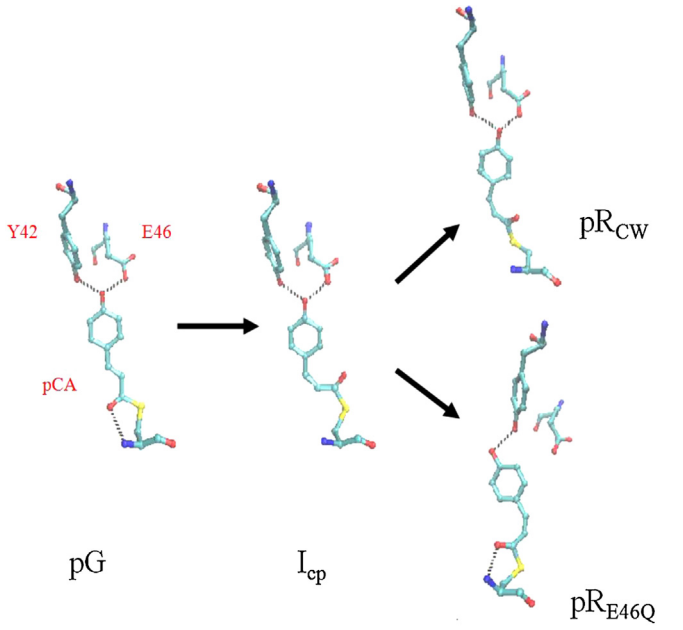

Fig. 10. First four deprotonated structures from transient X-ray diffraction experiments (PDB codes: 1TS0, 1TS7, 1TS8). In all four structures, the phenolate moiety is near planar with the double bond in the coumaryl tail indicating that conjugation has not been broken between the phenol conjugation system and the double bond bridge components (Table S2).

Braslavsky and coworkers estimated from photoacoustic measurements that the energy content of pR is 28 kcal/mol, which is approximately half of the nergy from 446-nm photons at the peak of PYP absorption spectrum [85]. The measured and calculated 0.6 pH upshift of the pK_a for the *cis* isomer pK_a corresponds to 1 kcal/mol energy difference (Eq. (1)), which is small compared to typical stabilities of proteins. However, Groenhof estimate a ΔG of for the protonation of *p*CA at 5 kcal/mol, which would be facilitated by the 20% decrease due to the *cis* conformation [25]. Photoreceptor proteins and signal transduction proteins, in general, are designed to take a stimulus (i.e., photon absorption) and couple it to a macroscopic deformation capable of propagation signal transduction in vivo; these proteins cannot be too strongly stabilized in deep energy wells.

Recently, Ihee et al. collected transient X-ray diffraction structures (PDB: 1TS0) and resolved three distinct structures adopted by the PYP chromophore after photoisomerization and before protonation (Fig. 10) and more states/structures were resolved after protonation [84]. Although their model involves a branching of kinetics that is not confirmed for solution phase kinetics of PYP, three states (pG, I_{cp}, pR_{cw} and pR_{E46}) exhibit *cis* configurations with similar and planar (±20°) conformational geometries (Table S2) to the dark-adapted structure (pG) with a *trans*-*p*CA configuration. Clearly, a simple two-state *cis*/*trans* geometry description is not applicable for the pre-protonated structures of PYP. Although the specific pK_a values for the twisted transient structure extracted from the time-resolved X-ray crystal studies are currently unknown (Fig. 10) [84], it is not unreasonable to expect similarly upshifted pK_a values compared to the pG state, as observed for the isolated *p*CA chromophore (Fig. 8). This requires a more complete ab initio study of each independent structure to understand how the pK_a is manipulated by chromophore geometry. This requires a higher-level theory than used here for *p*CA and TM*p*CA chromophore here, which takes into account the influence of the nearby residues in the chromophore binding pocket.

6. Concluding remarks

We explored the role that *cis* and *trans* configurations plays on manipulating the pK_a of the chromophore of Photoactive Yellow Protein (PYP) by investigating isolated para-coumaric acid (*p*CA) and thiomethyl-para-coumaric acid (TM*p*CA) models PYP chromophores in solution. UV illumination converts *p*CA from the *trans* to the *cis* form and the pK_a of the both conformers are resolved via pH titration coupled with electronic spectroscopy. The *cis* conformer exhibits a 0.6 pH unit higher pK_a than the *trans* form, which is directly compared to electronic structure calculations, which demonstrated how geometries and charge distributions. We rationalize that this higher pK_a originates from Columbic interactions between the phenolate and tail moieties, rather than changes in the conjugation backbone of the chromophore. Future work involves modeling the solvent explicitly using QM/MM(EFP) to compute pK_a values within Warshel's Linear response approximation in addition to computing ionization energies and excitation energies.

Acknowledgements

This work was supported with a Career Development Award (CDA0016/2007-C) from the Human Frontiers Science Program Organization to DSL and support from NSF grant: MCB-1051590. The computational part of this study was conducted under the auspices of the iOpenShell Center for Computational Studies of Electronic Structure and Spectroscopy of Open-Shell and Electronically Excited Species (http://iopenshell.usc.edu) supported by the National Science Foundation through the CRIF:CRF CHE-0625419+0624602+0625237 grant, as well as through the CHE-0951634 grant to AIK. We like to thank Dr. Scott Corley for aid in figures preparation.

Appendix A. Supplementary data

Supplementary data associated with this article can be found, in the online version, at http://dx.doi.org/10.1016/j.jphotochem.2013.06.019.

References

[1] B.L. Taylor, I.B. Zhulin, PAS domains: internal sensors of oxygen, redox potential, and light, Microbiology and Molecular Biology Reviews 63 (1999), 479-+.
[2] W.R. Briggs, J.L. Spudich, Handbook of Photosensory Receptors, Wiley-VCH Verlag GmbH & Co. KGaA, 2005.
[3] D. Hoersch, H. Otto, M.A. Cusanovich, M.P. Heyn, Time-resolved spectroscopy of dye-labeled photoactive yellow protein suggests a pathway of light-induced structural changes in the N-terminal cap, Physical Chemistry Chemical Physics 11 (2009) 5437–5444.
[4] M.A. van der Horst, K.J. Hellingwerf, Photoreceptor proteins, "star actors of modern times": a review of the functional dynamics in the structure of representative members of six different photoreceptor families, Accounts of Chemical Research 37 (2004) 13–20.
[5] A. Losi, Flavin-based blue-light photosensors: a photobiophysics update, Photochemistry and Photobiology 83 (2007) 1283–1300.
[6] W.W. Sprenger, W.D. Hoff, J.P. Armitage, K.J. Hellingwerf, The eubacterium ectothiorhodospira-halophila is negatively phototactic, with a wavelength dependence that fits the absorption-spectrum of the photoactive yellow protein, Journal of Bacteriology 175 (1993) 3096–3104.
[7] M.A. Cusanovich, T.E. Meyer, Photoactive yellow protein: a prototypic pas domain sensory protein and development of a common signaling mechanism, Biochemistry 42 (2003) 4759–4770.
[8] K.J. Hellingwerf, J. Hendriks, T. Gensch, Photoactive yellow protein, a new type of photoreceptor protein: will this "yellow lab" bring us where we want to go? Journal of Physical Chemistry A 107 (2003) 1082–1094.
[9] R. Kort, H. Vonk, X. Xu, W.D. Hoff, W. Crielaard, K.J. Hellingwerf, Evidence for trans–cis isomerization of the p-coumaric acid chromophore as the photochemical basis of the photocycle of photoactive yellow protein, FEBS Letters 382 (1996) 73–78.
[10] B. Perman, V. Srajer, Z. Ren, T. Teng, C. Pradervand, T. Ursby, D. Bourgeois, F. Schotte, M. Wulff, R. Kort, K. Hellingwerf, K. Moffat, Energy transduction on the nanosecond time scale: early structural events in a xanthopsin photocycle, Science 279 (1998) 1946–1950.

[11] U.K. Genick, S.M. Soltis, P. Kuhn, I.L. Canestrelli, E.D. Getzoff, Structure at 0.85 A resolution of an early protein photocycle intermediate, Nature 392 (1998) 206–209.
[12] U.K. Genick, G.E. Borgstahl, K. Ng, Z. Ren, C. Pradervand, P.M. Burke, V. Srajer, T.Y. Teng, W. Schildkamp, D.E. McRee, K. Moffat, E.D. Getzoff, Structure of a protein photocycle intermediate by millisecond time-resolved crystallography, Science 275 (1997) 1471–1475.
[13] M. Unno, M. Kumauchi, F. Tokunaga, S. Yamauchi, Vibrational assignment of the 4-hydroxycinnamyl chromophore in photoactive yellow protein, Journal of Physical Chemistry B 111 (2007) 2719–2726.
[14] D.H. Pan, A. Philip, W.D. Hoff, R.A. Mathies, Time-resolved resonance Raman structural studies of the pB′ intermediate in the photocycle of photoactive yellow protein, Biophysical Journal 86 (2004) 2374–2382.
[15] M. Unno, M. Kumauchi, N. Hamada, F. Tokunaga, S. Yamauchi, Resonance Raman evidence for two conformations involved in the L intermediate of photoactive yellow protein, Journal of Biological Chemistry 279 (2004) 23855–23858.
[16] M.A. van der Horst, J. Hendriks, J. Vreede, S. Yeremenko, W. Crielaard, K.J. Hellingwerf, Handbook of Photosensory Receptors, Wiley-VCH Verlag, Weinheim,Germany, 2005.
[17] J.H.K.J. Hellingwerf, M. van der Horst, A. Haker, W. Crielaard, T. Gensch, Photoreceptors and light signalling, comprehensive series in photochemistry and photobiology, The Royal Society of Chemistry 3 (2003).
[18] A. Xie, L. Kelemen, J. Hendriks, B.J. White, K.J. Hellingwerf, W.D. Hoff, Formation of a new buried charge drives a large-amplitude protein quake in photoreceptor activation, Biochemistry 40 (2001) 1510–1517.
[19] R. Brudler, R. Rammelsberg, T.T. Woo, E.D. Getzoff, K. Gerwert, Structure of the I1 early intermediate of photoactive yellow protein by FTIR spectroscopy, Natural Structural Biology 8 (2001) 265–270.
[20] A. Baltuška, I.H.M. van Stokkum, A. Kroon, R. Monshouwer, K.J. Hellingwerf, R. van Grondelle, The primary events in the photoactivation of yellow protein, Chemical Physics Letters 270 (1997) 263–266.
[21] T. Gensch, C.C. Gradinaru, I.H.M. van Stokkum, J. Hendricks, K. Hellingwerf, R. van Grondelle, The Primary photoreaction of photoactive yellow protein (PYP): anisotropy changes and excitation wavelength dependence, Chemical Physics Letters 356 (2002) 347.
[22] A. Xie, W.D. Hoff, A.R. Kroon, K.J. Hellingwerf, Glu46 donates a proton to the 4-hydroxycinnamate anion chromophore during the photocycle of photoactive yellow protein, Biochemistry 35 (1996) 14671–14678.
[23] H. Chosrowjan, N. Mataga, Y. Shibata, Y. Imamoto, F. Tokunaga, Environmental effects on the femtosecond-picosecond fluorescence dynamics of photoactive yellow protein: chromophores in aqueous solutions and in protein nanospaces modified by site-directed mutagenesis, Journal of Physical Chemistry B 102 (1998) 7695–7698.
[24] Y. Zhou, L. Ujj, T.E. Meyer, M.A. Cusanovich, G.H. Atkinson, Photocycle dynamics and vibrational spectroscopy of the E46Q mutant of photoactive yellow protein, Journal of Physical Chemistry A 105 (2001) 5719–5726.
[25] G. Groenhof, M.F. Lensink, H.J.C. Berendsen, A.E. Mark, Signal transduction in the photoactive yellow protein. II. Proton transfer initiates conformational changes, Proteins-Structure Function and Bioinformatics 48 (2002) 212–219.
[26] Y. Imamoto, K. Mihara, O. Hisatomi, M. Kataoka, F. Tokunaga, N. Bojkova, K. Yoshihara, Evidence for proton transfer from Glu-46 to the chromophore during the photocycle of photoactive yellow protein, Journal of Biological Chemistry 272 (1997) 12905–12908.
[27] T.E. Meyer, E. Yakali, M.A. Cusanovich, G. Tollin, Properties of a water-soluble, yellow protein isolated from a halophilic phototrophic bacterium that has photochemical activity analogous to sensory rhodopsin, Biochemistry 26 (1987) 418–423.
[28] W.D. Hoff, I.H.M. Vanstokkum, H.J. Vanramesdonk, M.E. Vanbrederode, A.M. Brouwer, J.C. Fitch, T.E. Meyer, R. Vangrondelle, K.J. Hellingwerf, Measurement and global analysis of the absorbency changes in the photocycle of the photoactive yellow protein from ectothiorhodospira-halophila, Biophysical Journal 67 (1994) 1691–1705.
[29] R. Marcus, Theoretical Relations among Rate Constants, Barriers, and Brønsted Slopes of Chemical Reactions, Journal of Pysical Chemistry 72 (1968) 891–899.
[30] R. Marcus, Unusual Slopes of free energy plots in kinetics, Journal of the American Chemical Society 91 (1969) 7224–7225.
[31] M.H. Andreas, D. Stahl, K. Singhal, I. van Stokkum, R. van Grondelle, M.L. Groot, K.J. Hellingwerf, On the involvement of single-bond rotation in the primary photochemistry of photoactive yellow protein, Biophysical Journal 101 (2011) 1184.
[32] I.B. Evgeniy, V. Gromov, H. Köppel, L.S. Cederbaum, Native hydrogen bonding network of the photoactive yellow protein (PYP) chromophore: impact on the electronic structure and photoinduced isomerization, Journal of Photochemistry and Photobiology A 234 (2012) 123.
[33] B.I.E.V. Gromov, H. Köppel, L.S. Cederbaum, Photoinduced isomerization of the photoactive yellow protein (PYP) chromophore: interplay of two torsions, a HOOP mode and hydrogen bonding, Journal of Physical Chemistry A 115 (2011) 9237.
[34] M.A.R. Martial Boggio-Pasqua, G. Groenhof, Hydrogen bonding controls excited-state decay of the photoactive yellow protein chromophore, Journal of the American Chemical Society 131 (2009) 13580.
[35] H.K. Misao Mizuno, M. Kataoka, Y. Mizutani, Changes in the hydrogen-bond network around the chromophore of photoactive yellow protein in the ground and excited states, Journal of Physical Chemistry B 115 (2011) 9306–9310.
[36] S. Hammes-Schiffer, A.A. Stuchebrukhov, Theory of coupled electron and proton transfer reactions, Chemical Reviews 110 (2010) 6939–6960.
[37] B. Borucki, Proton transfer in the photoreceptors phytochrome and photoactive yellow protein, Photochemical & Photobiological Sciences 5 (2006) 553–566.
[38] J.D. Chai, M. Head-Gordon, Systematic optimization of long-range corrected hybrid density functionals, Journal of Chemical Physics 128 (2008).
[39] F. Weinhold, NBO 5.0: new frontiers of localized analysis for NMR properties and transition metal bonding, Abstracts of Papers of the American Chemical Society 222 (2001) U195.
[40] Y. Shao, L.F. Molnar, Y. Jung, J. Kussmann, C. Ochsenfeld, S.T. Brown, A.T.B. Gilbert, L.V. Slipchenko, S.V. Levchenko, D.P. O'Neill, R.A. DiStasio Jr., R.C. Lochan, T. Wang, G.J.O. Beran, N.A. Besley, J.M. Herbert, C.Y. Lin, T. Van Voorhis, S.H. Chien, A. Sodt, R.P. Steele, V.A. Rassolov, P.E. Maslen, P.P. Korambath, R.D. Adamson, B. Austin, J. Baker, E.F.C. Byrd, H. Dachsel, R.J. Doerksen, A. Dreuw, B.D. Dunietz, A.D. Dutoi, T.R. Furlani, S.R. Gwaltney, A. Heyden, S. Hirata, C.-P. Hsu, G. Kedziora, R.Z. Khalliulin, P. Klunzinger, A.M. Lee, M.S. Lee, W. Liang, I. Lotan, N. Nair, B. Peters, E.I. Proynov, P.A. Pieniazek, Y.M. Rhee, J. Ritchie, E. Rosta, C.D. Sherrill, A.C. Simmonett, J.E. Subotnik, H.L. Woodcock III, W. Zhang, A.T. Bell, A.K. Chakraborty, D.M. Chipman, F.J. Keil, A. Warshel, W.J. Hehre, H.F. Schaefer III, J. Kong, A.I. Krylov, P.M.W. Gill, M. Head-Gordon, Advances in methods and algorithms in a modern quantum chemistry program package, Physical Chemistry Chemical Physics 8 (2006) 3172–3191.
[41] P. Changenet-Barret, P. Plaza, M.M. Martin, Primary events in the photoactive yellow protein chromophore in solution, Chemical Physics Letters 336 (2001) 439–444.
[42] P. Changenet-Barret, A. Espagne, N. Katsonis, S. Charier, J.-B. Baudin, L. Jullien, P. Plaza, M.M. Martin, Excited-state relaxation dynamics of a PYP chromophore model in solution: influence of the thioester group, Chemical Physics Letters 365 (2002) 285–291.
[43] K. Okamoto, N. Hamada, T. Sumi, T.-a. Okamura, N. Ueyama, H. Yamamoto, Investigation of the effect of the NH center dot center dot center dot OC Hydrogen Bond from Cys69 to PYP chromophore using novel active-center model compound, Chemistry Letters 38 (2009) 456–457.
[44] K. Okamoto, N. Hamada, T.-a. Okamura, N. Ueyama, H. Yamamoto, Color regulation and stabilization of chromophore by Cys69 in photoactive yellow protein active center, Organic & Biomolecular Chemistry 7 (2009) 3782–3791.
[45] J. Berna, A.M. Brouwer, S.M. Fazio, N. Haraszkiewicz, D.A. Leigh, C.M. Lennon, A rotaxane mimic of the photoactive yellow protein chromophore environment: effects of hydrogen bonding and mechanical interlocking on a coumaric amide derivative, Chemical Communications (2007) 1910–1912.
[46] J.J. van Thor, A.J. Pierik, I. Nugteren-Roodzant, A.H. Xie, K.J. Hellingwerf, Characterization of the photoconversion of green fluorescent protein with FTIR spectroscopy, Biochemistry 37 (1998) 16915–16921.
[47] M. Vengris, D.S. Larsen, M.A. van der Horst, O.F.A. Larsen, K.J. Hellingwerf, R. van Grondelle, Ultrafast dynamics of isolated model photoactive yellow protein chromophores: "chemical perturbation theory" in the laboratory, Journal of Physical Chemistry B 109 (2005) 4197–4208.
[48] I. Polyakov, E. Epifanovsky, B. Grigorenko, A.I. Krylov, A. Nemukhin, Quantum chemical benchmark studies of the electronic properties of the green fluorescent protein chromophore: 2. Cis–trans isomerization in water, Journal of Chemical Theory and Computation 5 (2009) 1907–1914.
[49] D. Zuev, K.B. Bravaya, T.D. Crawford, R. Lindh, A.I. Krylov, Electronic structure of the two isomers of the anionic form of p-coumaric acid chromophore, Journal of Chemical Physics 134 (2011).
[50] D.S. Larsen, M. Vengris, I.H.M. van Stokkum, M.A. van der Horst, F.L. de Weerd, K.J. Hellingwerf, R. van Grondelle, Photoisomerization and photoionization of the photoactive yellow protein chromophore in solution, Biophysical Journal 86 (2004) 2538–2550.
[51] L.L. Premvardhan, F. Buda, M.A. van der Horst, D.C. Luhrs, K.J. Hellingwerf, R. van Grondelle, Impact of photon absorption on the electronic properties of p-coumaric acid derivatives of the photoactive yellow protein chromophore, Journal of Physical Chemistry B 108 (2004) 5138–5148.
[52] G. Aulinerd, R. Sanden, Spectrographic contributions to lignin chemistry. 9. Absorption properties of some 4-hydroxyphenyl guaiacyl and 4-hydroxy-3,5-dimethoxyphenyl type model compounds for hardwood lignins, Acta Chemica Scandinavica 22 (1968), 1187-&.
[53] O. Tchaikovskaya, I. Sokolova, N. Sultimova, G. Mayer, The effect of UV radiation on the phenol photodegradation in the presence of humic and fulvic acids, Proceedings of SPIE – International Society for Optical Engineering 5743 (2004) 156–160.
[54] J. Hendriks, K.J. Hellingwerf, pH dependence of the photoactive yellow protein photocycle recovery reaction reveals a new late photocycle intermediate with a deprotonated chromophore, Journal of Biological Chemistry 284 (2009) 5277–5288.
[55] M.K. Gilson, J.A. Given, B.L. Bush, J.A. McCammon, The statistical-thermodynamic basis for computation of binding affinities: a critical review, Biophysical Journal 72 (1997) 1047–1069.
[56] S.C.L. Kamerlin, M. Haranczyk, A. Warshel, Progress in ab initio QM/MM free-energy simulations of electrostatic energies in proteins: accelerated QM/MM studies of p*K*(a), redox reactions and solvation free energies, Journal of Physical Chemistry B 113 (2009) 1253–1272.
[57] J.H. Jensen, H. Li, A.D. Robertson, P.A. Molina, Prediction and rationalization of protein p*K*(a) values using QM and QM/MM methods, Journal of Physical Chemistry A 109 (2005) 6634–6643.

[58] D. Riccardi, P. Schaefer, Q. Cui, pK(a) calculations in solution and proteins with QM/MM free energy perturbation simulations: a quantitative test of QM/MM protocols, Journal of Physical Chemistry B 109 (2005) 17715–17733.
[59] A.V. Marenich, C.J. Cramer, D.G. Truhlar, Performance of SM6, SM8, and SMD on the SAMPL1 test set for the prediction of small-molecule solvation free energies, Journal of Physical Chemistry B 113 (2009) 4538–4543.
[60] D.M. Chipman, Reaction field treatment of charge penetration, Journal of Chemical Physics 112 (2000) 5558.
[61] E. Cancès, B. Mennucci, J. Tomasi, A new integral equation formalism for the polarizable continuum model: Theoretical background and applications to isotropic and anisotropic dielectrics, Journal of Chemical Physics 107 (1997) 3032.
[62] T.N. Truong, E.V. Stefanovich, Analytical first and second energy derivatives of the generalized conductor-like screening model for free energy of solvation, Journal of Computational Chemistry 103 (1995) 3709.
[63] M. Cossi, N. Rega, V. Scalmani, G. Barone, universal approach to solvation modeling, Accounts of Chemical Research 41 (2008) 760.
[64] C.J. Cramer, D.G. Truhlar, A universal approach to solvation modeling, Accounts of Chemical Research 41 (2008) 760.
[65] M.H. Cohen, A.D. Earhart, J.V. Coe, T.R. Tuttle, The proton's absolute aqueous enthalpy and gibbs free energy of solvation from cluster-ion solvation data, Journal of Physical Chemistry A 102 (1998) 7787.
[66] J. Knowles, The intrinsic pK_a-values of functional groups in enzymes: improper deductions from the pH-dependence of steady-state parameters, CRC Critical Reviews in Biochemistry 4 (1976) 165–173.
[67] A. Fersht, Structure and Mechanism in Protein Science: A Guide to Enzyme Catalysis and Protein Folding, W.H. Freeman & Co., New York, 1999.
[68] J.E. Nielsen, J.A. McCammon, Calculating pK_a values in enzyme active sites, Protein Science 12 (2003) 1894–1901.
[69] M. Putschogl, P. Zirak, A. Penzkofer, Absorption and emission behaviour of trans-p-coumaric acid in aqueous solutions and some organic solvents, Chemical Physics 343 (2008) 107–120.
[70] S. Al Arni, A.F. Drake, M. Del Borghi, A. Converti, Study of aromatic compounds derived from sugarcane bagasse. Part I: effect of pH, Chemical Engineering & Technology 33 (2010) 895–901.
[71] P. Changenet-Barret, A. Espagne, S. Charier, J.B. Baudin, L. Jullien, P. Plaza, K.J. Hellingwerf, M.M. Martin, Early molecular events in the photoactive yellow protein: role of the chromophore photophysics, Photochemical & Photobiological Sciences 3 (2004) 823–829.
[72] W.D. Hoff, I.H.M. Van Stokkum, J. Gural, K.J. Hellingwerf, Comparison of acid denaturation and light activation in the eubacterial blue-light receptor photoactive yellow protein, Biochimica et Biophysica Acta 1322 (1997) 151–162.
[73] W.D. Hoff, A. Xie, I.H.M. Van Stokkum, X.J. Tang, J. Gural, A.R. Kroon, K.J. Hellingwerf, Global conformational changes upon receptor stimulation in photoactive yellow protein, Biochemistry 38 (1999) 1009–1017.
[74] Y. Imamoto, M. Harigal, M. Kataoka, Direct observation of the pH-dependent equilibrium between L-like and M intermediates of photoactive yellow protein, FEBS Letters 577 (2004) 75–80.
[75] H. Kamikubo, T. Koyama, M. Hayashi, K. Shirai, Y. Yamazaki, Y. Imamoto, M. Kataoka, The photoreaction of the photoactive yellow protein domain in the light sensor histidine kinase Ppr is influenced by the C-terminal domains, Photochemistry and Photobiology 84 (2008) 895–902.
[76] A. Warshel, Bicycle-pedal model for 1st step in vision process, Nature 260 (1976) 679–683.
[77] S. Braun-Sand, P.K. Sharma, Z.T. Chu, A.V. Pisliakov, A. Warshel, The energetics of the primary proton transfer in bacteriorhodopsin revisited: it is a sequential light-induced charge separation after all, Biochimica et Biophysica Acta 1777 (2008) 441–452.
[78] U. Zadok, A. Khatchatouriants, A. Lewis, M. Ottolenghi, M. Sheves, Light-induced charge redistribution in the retinal chromophore is required for initiating the bacteriorhodopsin photocycle, Journal of the American Chemical Society 124 (2002) 11844–11845.
[79] R. Cordfunke, R. Kort, A. Pierik, B. Gobets, G.-J. Koomen, J.W. Verhoeven, K.J. Hellingwerf, Trans/cis (Z/E) photoisomerization of the chromophore of photoactive yellow protein is not a prerequisite for the initiation of the photocycle of this photoreceptor protein, Proceedings of the National Academy of Sciences of the United States of America 95 (1998) 7396–7401.
[80] A.R. Kroon, W.D. Hoff, H.P. Fennema, J. Gijzen, G.J. Koomen, J.W. Verhoeven, W. Crielaard, K.J. Hellingwerf, Spectral tuning, fluorescence, and photoactivity in hybrids of photoactive yellow protein, reconstituted with native or modified chromophores, Journal of Biological Chemistry 271 (1996) 31949–31956.
[81] D.S. Larsen, M. Vengris, I.H.M. van Stokkum, M. van der Horst, F.L. de Weerd, K.J. Hellingwerf, R. van Grondelle, Photoisomerization and photoionization of the photoactive yellow protein chromophore in solution, Biophysical Journal 86 (2004) 2538–2550.
[82] M.E. Vanbrederode, T. Gensch, W.D. Hoff, K.J. Hellingwerf, S.E. Braslavsky, Photoinduced volume change and energy-storage associated with the early transformations of the photoactive yellow protein from ectothiorhodospira-halophila, Biophysical Journal 68 (1995) 1101–1109.
[83] M. Yoda, Y. Inoue, M. Sakurai, Effect of protein environment on pK(a) shifts in the active site of photoactive yellow protein, Journal of Physical Chemistry B 107 (2003) 14569–14575.
[84] H. Ihee, S. Rajagopal, V. Srajer, R. Pahl, S. Anderson, M. Schmidt, F. Schotte, P.A. Anfinrud, M. Wulff, K. Moffat, Visualizing reaction pathways in photoactive yellow protein from nanoseconds to seconds, Proceedings of the National Academy of Sciences of the United States of America 102 (2005) 7145–7150.
[85] M.E. van Brederode, T. Gensch, W.D. Hoff, K.J. Hellingwerf, S.E. Braslavsky, Photoinduced volume change and energy storage associated with the early transformations of the photoactive yellow protein from *Ectothiorhodospira halophila*, Biophysical Journal 68 (1995) 1101–1109.